Electronic Supplementary Information (ESI)

MOF-derived Bi@NC electrocatalysts with heteroatomic engineering for high-efficiency CO_2-to-formate conversion

Jingxuan Song,[‡a,] Yuexian Du,[‡a] Lu Liu,[a] Kunfan Dong,[a] Ziyu Deng,[a] Yanghe Fu,*[a] Yijing Gao,*[a] Fumin Zhang,[a] Fa Yang,*[a] Weidong Zhu*[a] and Maohong Fan[b]

[a] *Key Laboratory of the Ministry of Education for Advanced Catalysis Materials, Zhejiang Engineering Laboratory for Green Syntheses and Applications of Fluorine-Containing Specialty Chemicals, Zhejiang Normal University, Jinhua 321004, China*

[b] *College of Engineering and Physical Sciences, School of Energy Resources, University of Wyoming, Laramie, WY 82071, USA*

[‡] These authors contributed equally to this work.

[*]Corresponding authors:

E-mail addresses: yhfu@zjnu.cn (Y. Fu), yijinggao@zjnu.edu.cn (Y. Gao), yangfa@zjnu.edu.cn (F. Yang), and weidongzhu@zjnu.cn (W. Zhu).

Table of contents entry

1 Experimental and computational methods

1.1. Reagents

Ellagic acid (96 wt%) and bismuth acetate (99 wt%) were purchased from Shanghai Macklin Biochemical Technology Co., Ltd. Dicyandiamide was purchased from Shanghai Meryer Chemical Technology Co., Ltd. Potassium bicarbonate ($KHCO_3$), acetic acid, and ethanol were purchased from Sinopharm Chemical Reagent Co., Ltd. The carbon paper (TGP-H-060) was purchased from Toray. Nafion (5 wt%) and Nafion 117 membrane were purchased from Dupont. All reagents of analytical reagent grade were used as received without further purification.

1.2. Characterizations

Powder X-ray diffraction (XRD) measurements were performed using a Bruker D8 Advance X-ray diffractometer with Cu *Kα* radiation. Scanning electron microscope (SEM) with energy dispersive X-ray spectroscopy (EDX) was carried out by a GeminiSEM300. The morphology and internal structure were observed by JEM-2100F transmission electron microscope (TEM) with an accelerating voltage of 200 kV. The surface composition of the samples was determined by a ThermoFisher Scientific EscaLab 250 Xi X-ray photoelectron spectroscopy (XPS) using Al *Kα* radiation. The N_2 adsorption-desorption isotherms at 77 K were performed to determine the Brunauer-Emmett-Teller (BET) surface area (S_{BET}) using an ASAP 2020 physical adsorption instrument (Micromeritics Instrument Corp.), which was also for CO_2 adsorption measurements at 298 K. Raman spectra

of the as-prepared catalysts were determined by a Raman spectrometer (Horiba HR Evolution, 532 nm). Elemental analysis (EA) for C and N was performed on an Elementar Vario EL cube elemental analyzer. The amounts of Bi for the prepared samples were determined using a ThermoFisher iCAP 7400 inductive coupled plasma optical emission spectrometer (ICP-OES).

1.3. Electrochemical measurements

The electrochemical measurements were performed with a CHI 760E workstation (Shanghai Chenhua Instruments Co.) in a typical three-electrode system with a sample-coated carbon paper, Ag/AgCl electrode and Pt plate served as the working electrode, the reference electrode, and the counter electrode, respectively. The working electrode was prepared as follows: 5 mg of the prepared catalyst was added into the mixture of ethanol/H_2O (150 μL, 1:2 in v/v) and Nafion solution (50 μL, 3 wt%). After sonicating for 30 min to get a uniform ink, 10 μL of the obtained ink was evenly dropped on carbon paper with an area of 0.5 cm × 0.5 cm, and the loading density of the catalyst was about 1.0 mg cm^{-2}. A standard H-type cell was used as the electrolyzer using Nafion 117 membrane as the separator, in which $KHCO_3$ aqueous solution (0.5 M) was used as the electrolyte. Before performing electrochemical measurements, the electrolyte was purged with N_2 to remove the dissolved O_2, and then flowed with CO_2 till saturation. 20 cycles of cyclic voltammetry (CV) sweeps were conducted before linear sweep voltammetry (LSV) curves were collected at a scanning rate of 10 mV s^{-1} with CO_2 bubbling. During the constant voltage test, CO_2 was delivered into the

chamber of the working electrode with a flow rate of 10 mL min^{-1}. All the potentials were calibrated to the reversible hydrogen electrode (RHE) by the equation: $E_{RHE} = E_{Ag/AgCl} + 0.0592 \times pH + 0.197$ V.

The electrochemical active surface area (ECSA) of the prepared catalyst was approximately estimated through the electrochemical double-layer capacitance (C_{dl}). In a non-Faradaic potential range, the CV curves were separately recorded in a single cell with a scan rate of 20, 40, 60, 80, 100, or 120 mV s^{-1}. A fitted linear line was then obtained by plotting the difference in current density between anodic and cathodic sweeps against the scan rate, and the slope of the fitting line represented C_{dl}. ECSA was estimated using the equation: ECSA = C_{dl}/C_s, where C_s represented the average specific capacitance and the value was 20 μF cm^{-2}. The electrochemical impedance spectroscopy (EIS) was performed in the frequency range of 10^{-1}-10^5 Hz at a voltage of −0.8 V *vs*. RHE with an amplitude of 5.0 mV.

1.4. Computational methods

The Vienna *ab*-initio Simulation Package (VASP) was used for density functional theory (DFT) calculations.[1] The Perdew-Burke-Ernzerhof (PBE) functional of generalized gradient approximation (GGA) was used to describe the electron exchange correlation energy,[2] and the Projector Augmented Wave (PAW) method was used to describe the interaction between electrons and ions.[3] The cutoff energy was set to 450 eV. The K-point used in optimization was 3 × 3 × 1.[4] The convergence criteria for energy and force were 1 × 10^{-5} eV and -0.01 eV/Å, respectively. The van der Waals (vdW) interaction was described by using DFT-D3 method.[5] To prevent interaction

between adjacent layers, the height of the vacuum layer along the *z* direction was set as 15 Å. The charge density difference was analyzed using VESTA software.[6]

The adsorption energy (E_{ad}) of CO_2 was calculated as follows:

$$E_{ad} = E_{total} - E_{gas} - E_{catal}$$

where E_{total} is the total energy of CO_2 adsorbed on the catalyst, E_{gas} is the gaseous energy of CO_2, and E_{catal} is the energy of Bi@NC or Bi@C.

Based on the computational hydrogen electrode (CHE) model proposed by Nørskov et al.,[7] the change of free energy (ΔG) for each elementary reaction step in the CO_2RR process was calculated by follow equation:[8]

$$\Delta G = \Delta E + \Delta E_{ZPE} - T\Delta S$$

where ΔE is the total energy, ΔE_{ZPE} is the zero-point energy (ZPE) correction based on the calculated vibrational frequency, $T\Delta S$ is the entropy contribution at T = 298.15 K. In addition, the free energy of $H^+ + e^-$ is equal to 1/2 H_2.

2 Figures and tables

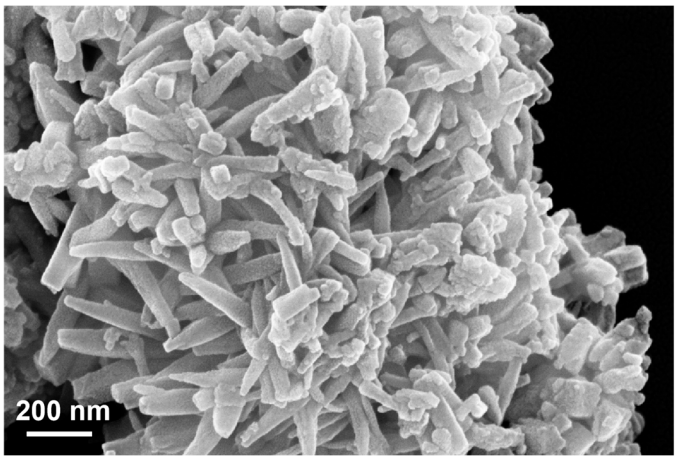

Fig. S1. SEM image of Bi-MOF.

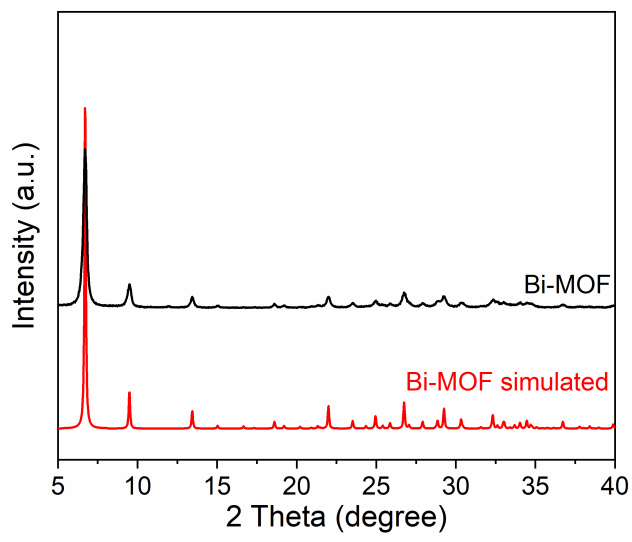

Fig. S2. XRD patterns of the as-synthesized and the simulated Bi-MOF.

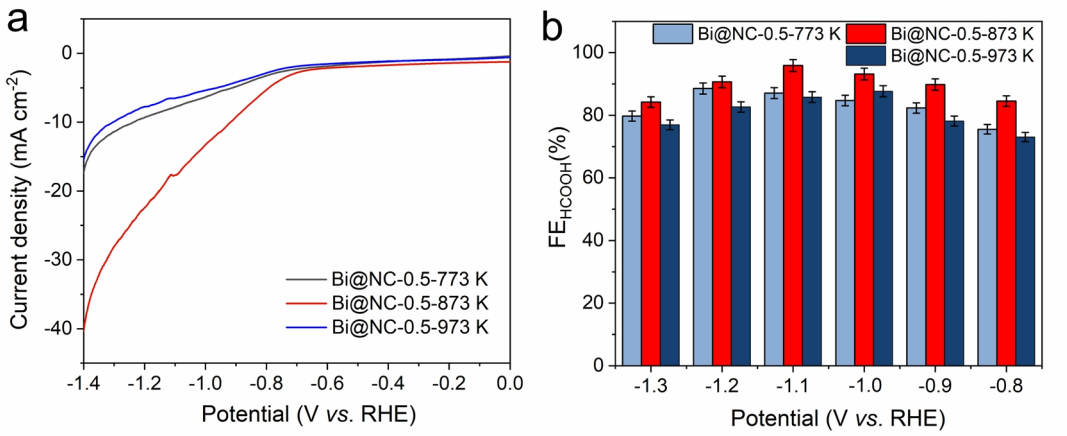

Fig. S3. LSV curves (a) and FE_{HCOOH} (b) of Bi@NC-0.5 at pyrolysis temperatures of 773, 873, and 973 K.

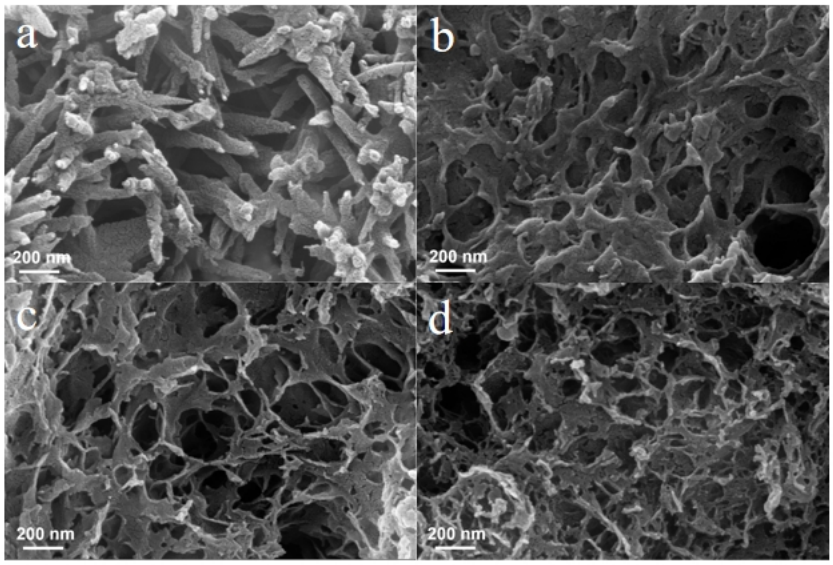

Fig. S4. SEM images of Bi@C (a) and Bi@NC-*x* (*x* = 0.3, 0.5, and 0.7) (b-d).

Table S1. Elemental contents of Bi, C, N, and O in Bi@C and Bi@NC

Sample	Bi (wt%)[a]	C (wt%)[b]	N (wt%)[b]	O (wt%)[b]
Bi@C	52.7	40.1	-	6.8
Bi@NC-0.3	52.4	25.0	15.7	4.9
Bi@NC-0.5	53.3	25.0	16.9	4.5
Bi@NC-0.7	52.2	25.7	17.4	4.1

[a] Detected by ICP-OES; [b] detected by EA.

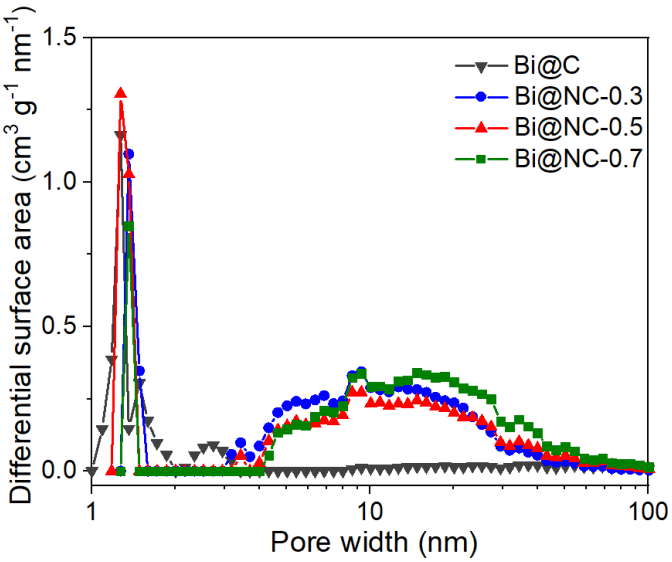

Fig. S5. Pore size distributions of Bi@C and Bi@NC.

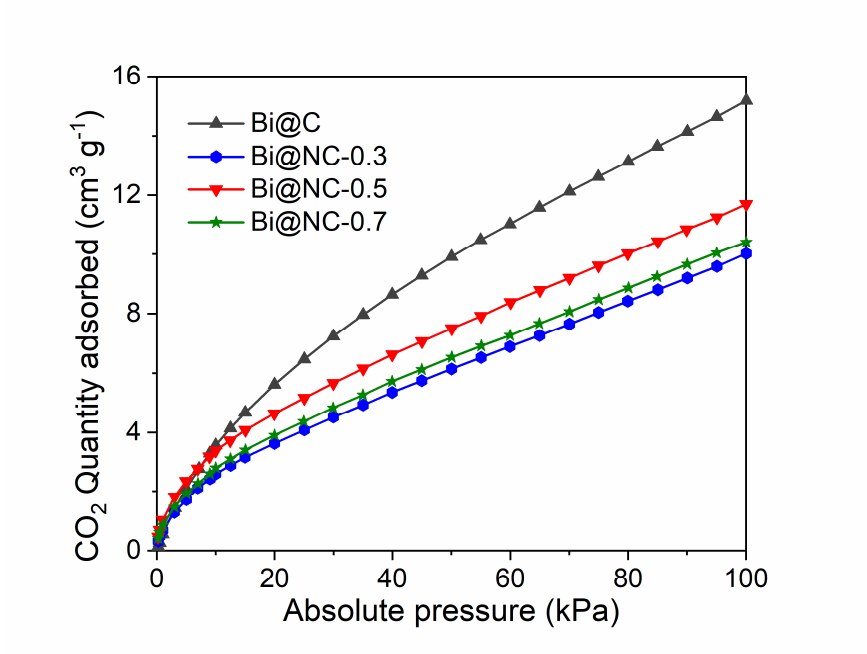

Fig. S6. Adsorption of CO_2 on Bi@C and Bi@NC at 298 K.

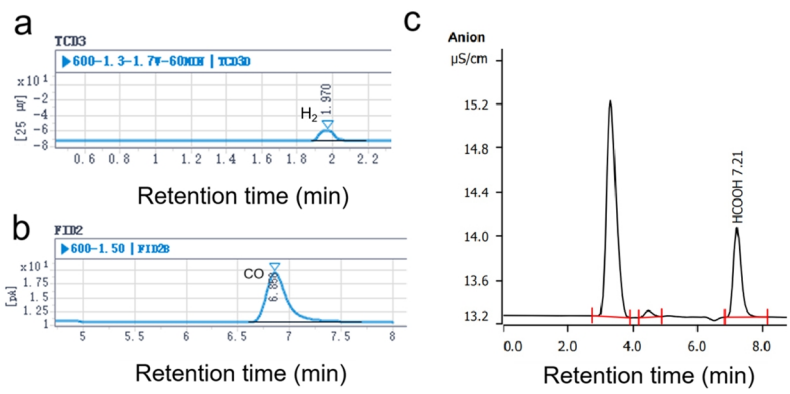

Fig. S7. Analytical chromatograms of generated products: H_2 (a) and CO (b) via gas chromatography, and HCOOH (c) via ion chromatography.

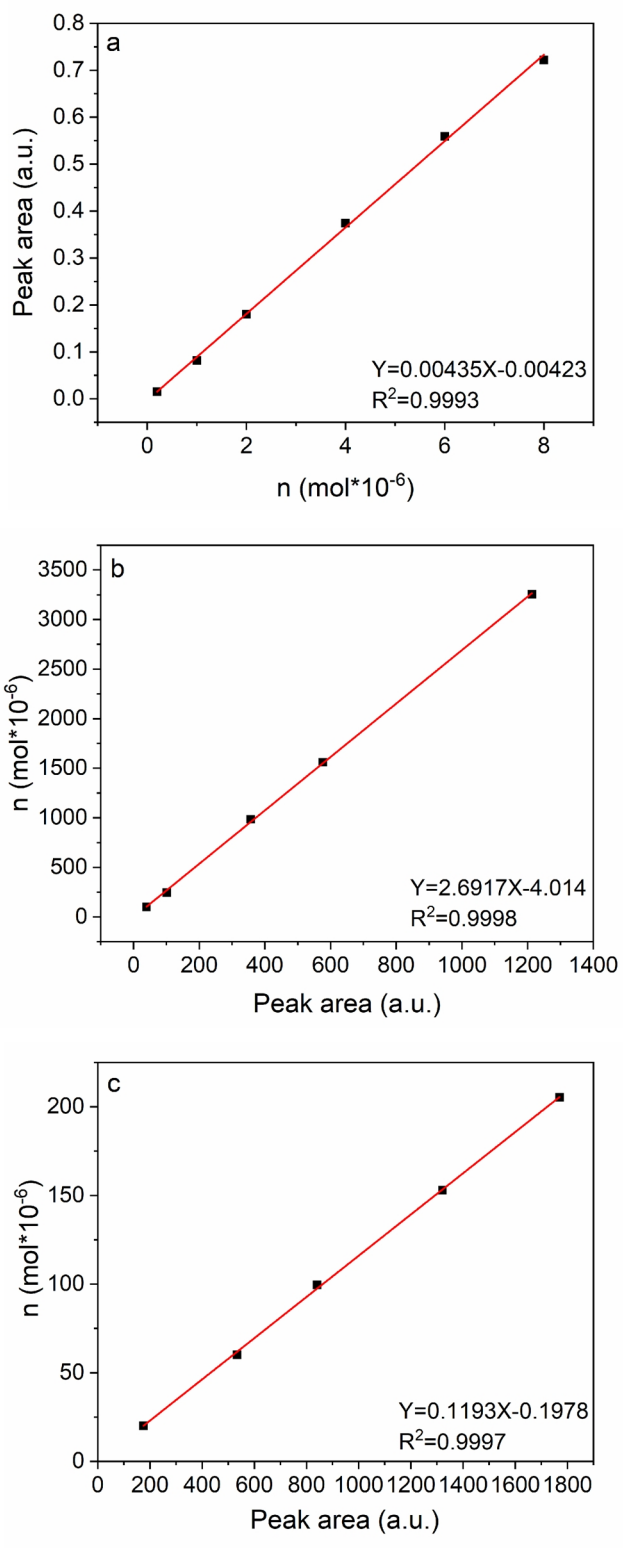

Fig. S8. Standard calibrated curves for determining the amounts of the yielded HCOOH (a), H_2 (b), and CO (c).

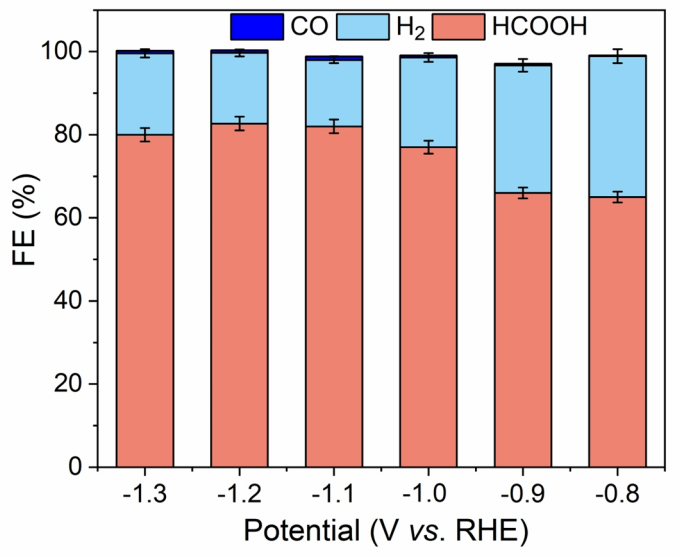

Fig. S9. FEs of HCOOH, H_2 and CO towards Bi-MOF for eCO_2R reaction in an H-cell electrolyzer.

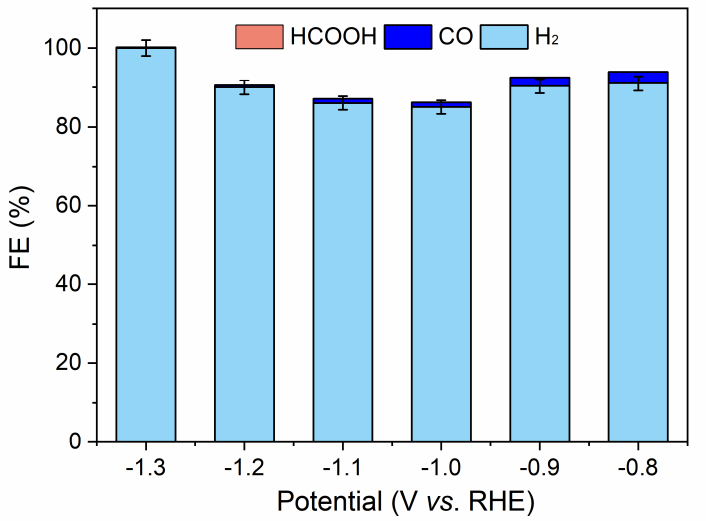

Fig. S10. FEs of HCOOH, H_2 and CO in eCO_2R reaction using NC as the catalyst in an H-cell.

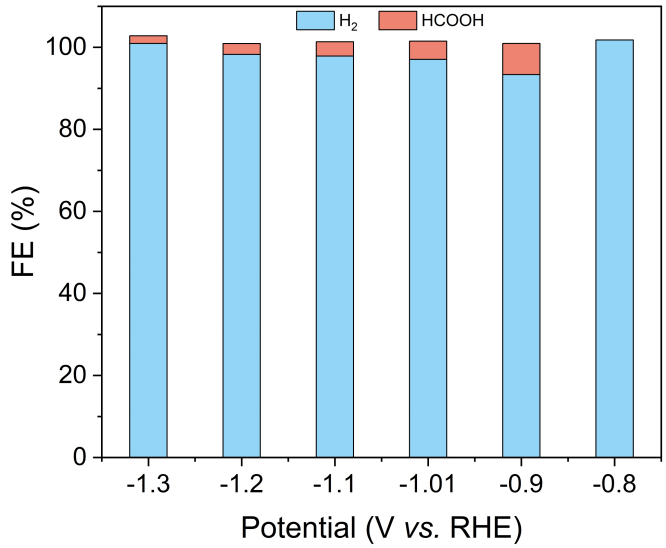

Fig. S11. FEs of HCOOH and H_2 CO under Ar atmosphere using Bi@NC-0.5 as the catalyst in an H-cell.

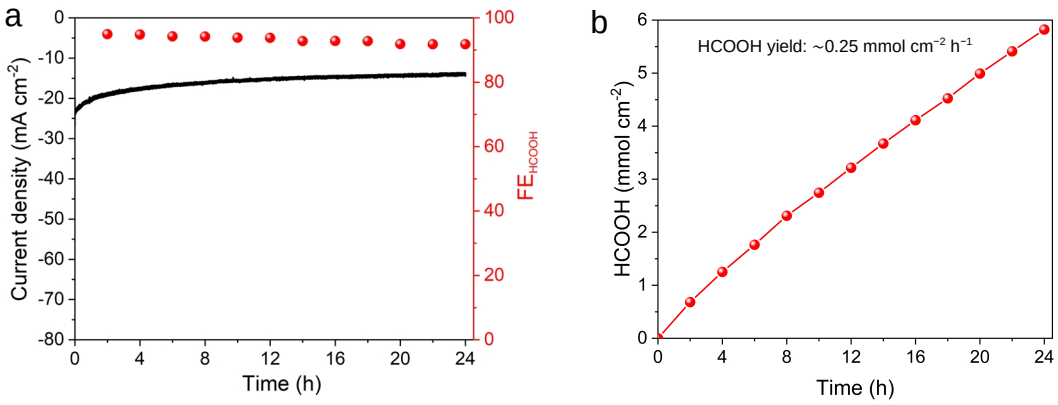

Fig. S12. Long-term stability of Bi@NC-0.5 for eCO_2R in an H-cell electrolyzer: current density, FE (a), and production rate (b) of HCOOH.

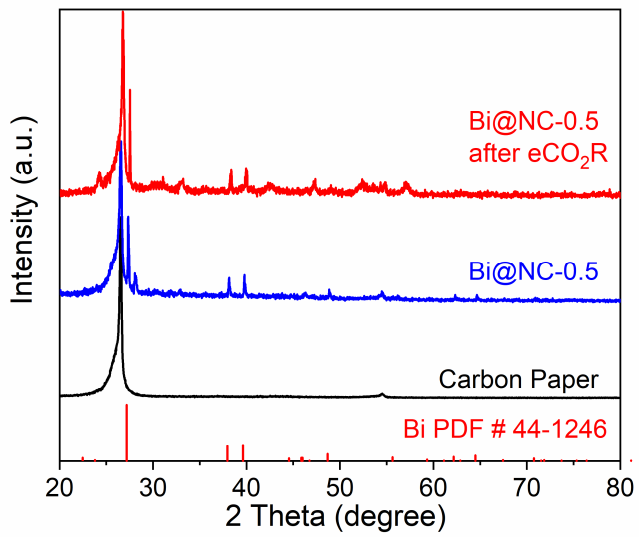

Fig. S13. XRD patterns of Bi@NC-0.5 before and after eCO_2R.

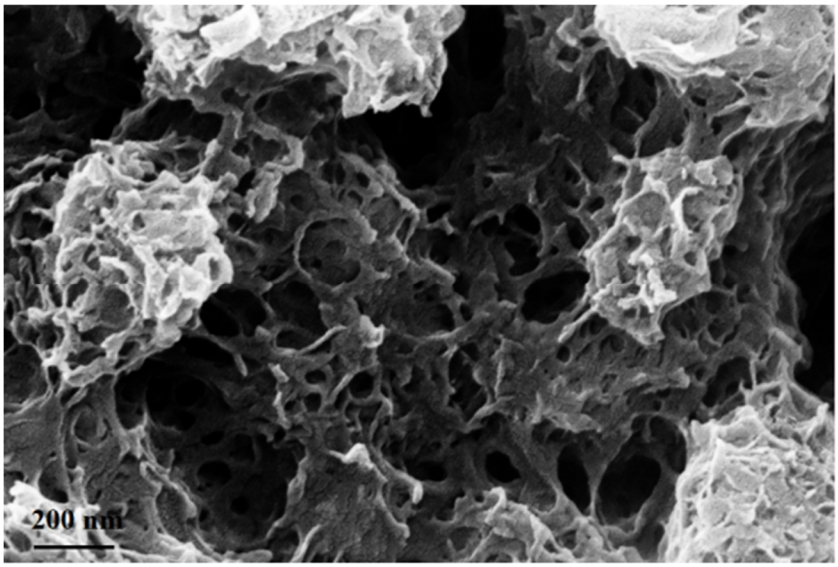

Fig. S14. SEM image of the used Bi@NC-0.5 after eCO_2R.

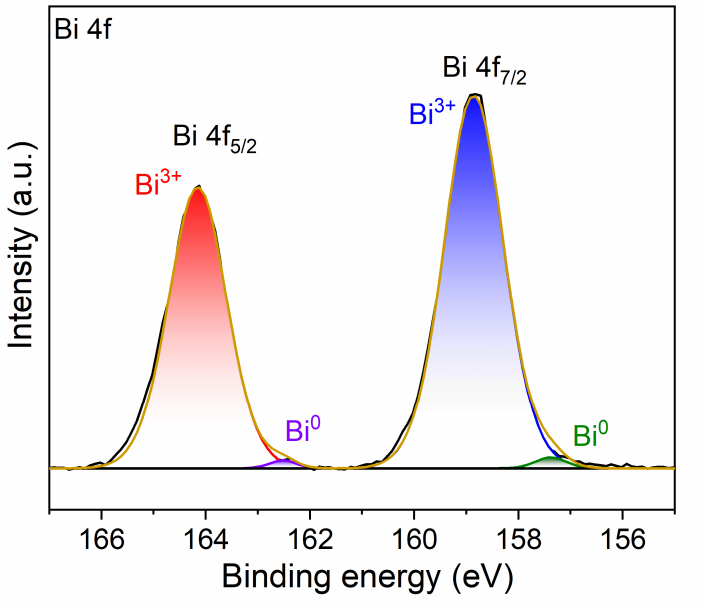

Fig. S15. XPS spectrum of the used Bi@NC-0.5 after eCO_2R.

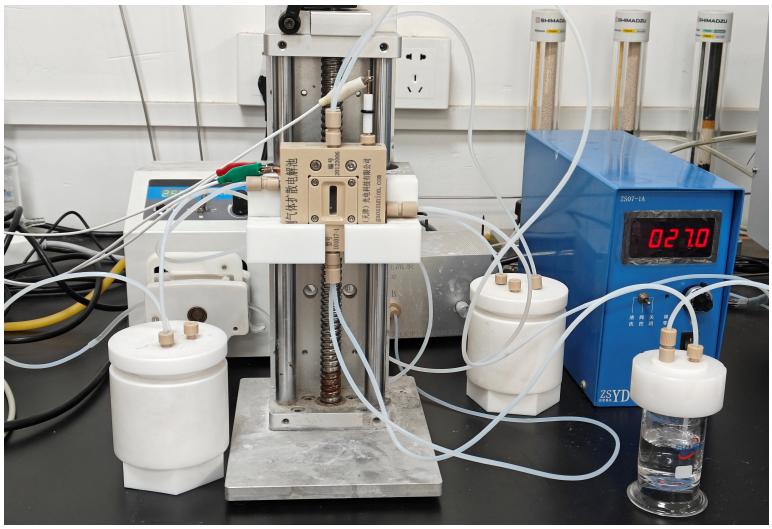

Fig. S16. eCO_2R reaction in a flow-cell setup.

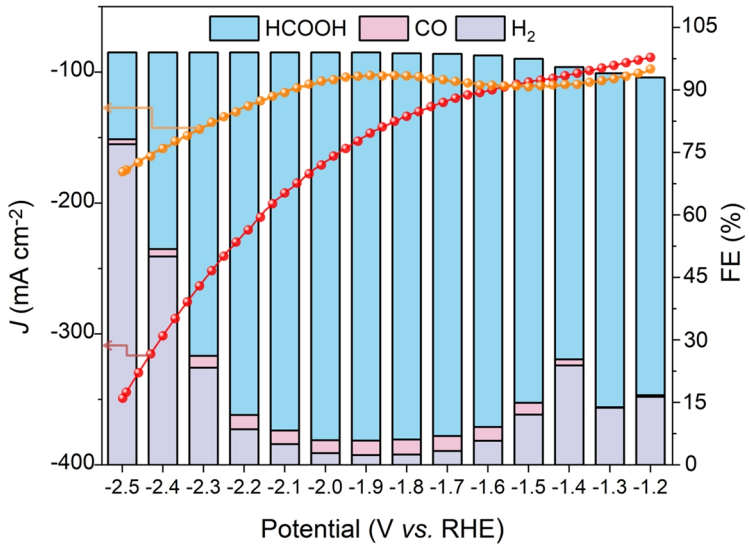

Fig. S17. eCO_2R performance of Bi@NC-0.5 in a flow cell setup: LSV curves in N_2 (yellow) and CO_2 (red), and FEs for H_2, CO, and HCOOH.

Table S2. Performance comparison of Bi-based catalysts for eCO_2R in an H-type cell

Catalyst	Electrolyte	FE_{HCOOH} (%)	J_{HCOOH} (mA cm^{-2})	Ref.
Bi@NC–0.5	0.5 M $KHCO_3$	96.0 (−1.1 V)	−16.4 (−1.1 V)	This work
SOR Bi@C NPs	0.5 M $KHCO_3$	95.0 (−1.0 V)	−10.5 (−1.0 V)	9
PNCB	0.5 M $KHCO_3$	94.8 (−1.05 V)	−22.0 (−1.05V)	10
Bi–D	0.5 M $KHCO_3$	93.9 (−0.9 V)	−10.0 (−1.0 V)	11
CT–hBiOBr	0.5 M $KHCO_3$	90.0 (−0.7 V)	−100.0 (−0.7 V)	12
CeOx/Bi	0.1 M $KHCO_3$	91.1 (−0.9 V)	16.1 (−0.9 V)	13
PD–Bi1	0.5 M $KHCO_3$	91.4 (−0.9 V)	−6.5 (−0.9 V)	14
2D Bi	0.5 M $KHCO_3$	90 (−0.84 V)	−18.7 (−0.84 V)	15
Bi–Sb	0.5 M $KHCO_3$	88.3 (−0.9 V)	−8.52 (−0.9 V)	16
Bi LNSs	1 M $KHCO_3$	94.3 (−0.76 V)	−31 (−0.76 V)	17
Bi NPs–C60 NS	0.5 M $KHCO_3$	94.31 (−1.0 V)	−88.29 (−1.0 V)	18
SAC Bi@C–600	0.1 M $KHCO_3$	88 (−1.5 V)	−12 (−1.5 V)	19
Bi–MOF	0.5 M $KHCO_3$	94.3 (−1.08 V)	−20 (−1.08 V)	20

BiMOF–NC	0.1 M $KHCO_3$	~100 (−1.2 V)	-27.9 (−1.2 V)	21
Bi–MOF derived CPBC	0.1 M $KHCO_3$	~100 (−0.7 V)	~4 (−0.7 V)	22
Bi–NFs	0.1 M $KHCO_3$	92.3 (−0.9 V)	28.5 (−1.05 V)	23
Bi-ZMOF	0.1 M $KHCO_3$	91 (−1.1 V)	15 (−1.3 V)	24

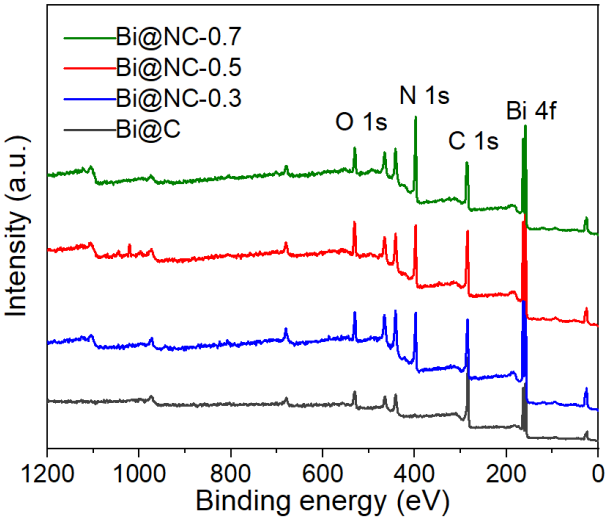

Fig. S18. Full XPS spectra of Bi@C and Bi@NC.

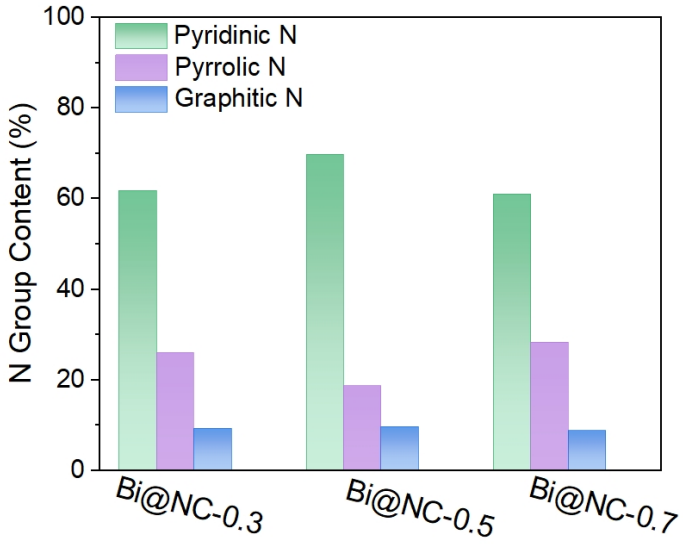

Fig. S19. Contents of pyridinic, pyrrolic, and graphitic N in Bi@NC.

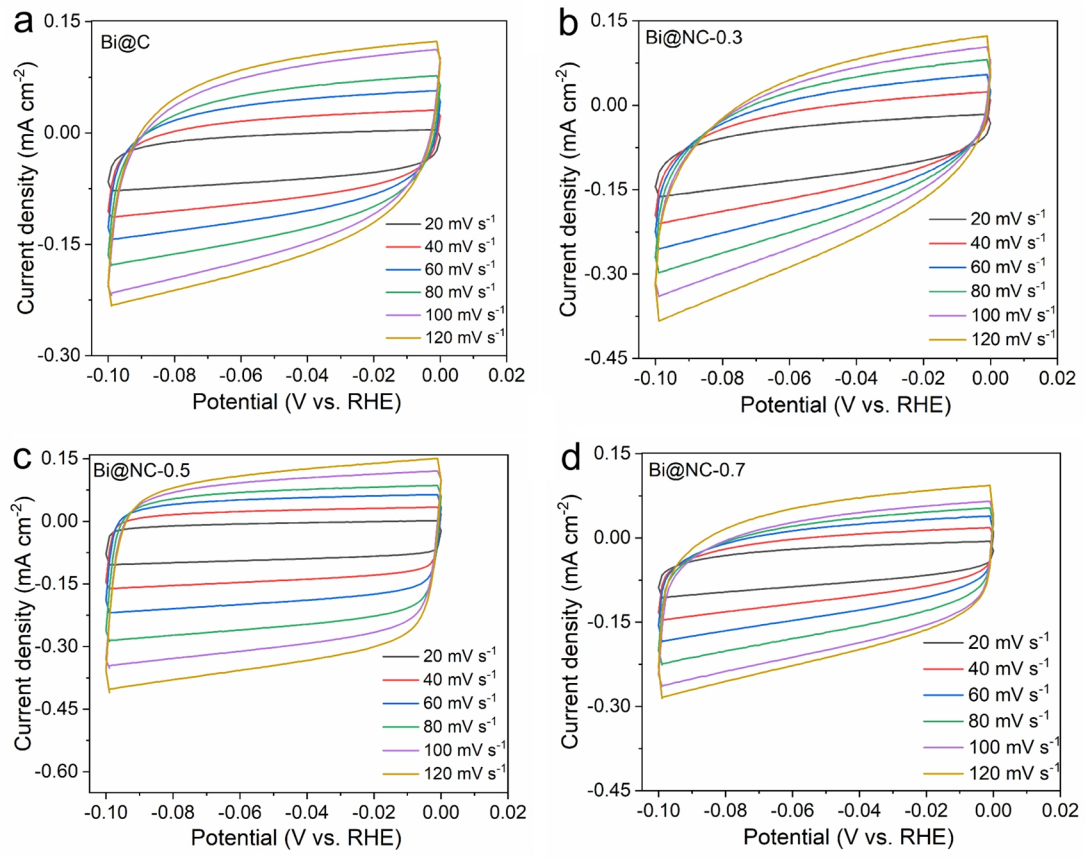

Fig. S20. CV curves at different scan rates of Bi@C (a), Bi@NC-0.3 (b), Bi@NC-0.5 (c), and Bi@NC-0.7 (d).

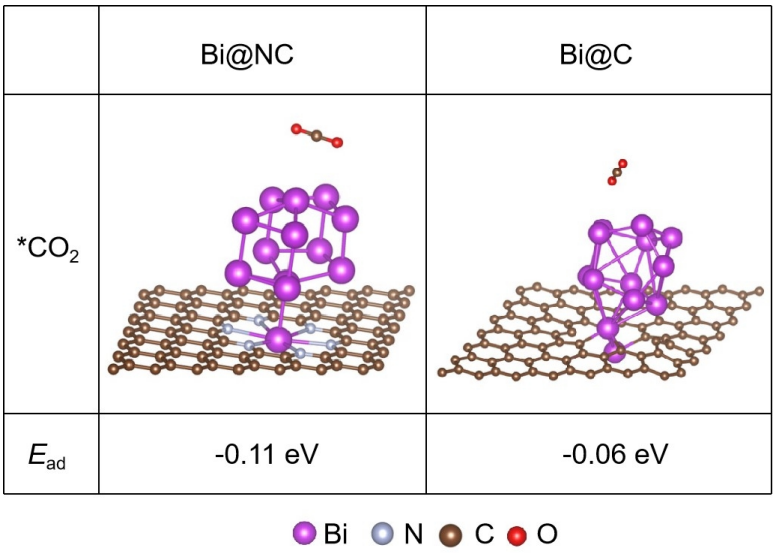

Fig. S21. Optimal structures and E_{ad} of CO_2 adsorbed on Bi@C and Bi@NC.

	*COOH	*H_2O+*CO	*HCOOH
CONTCAR	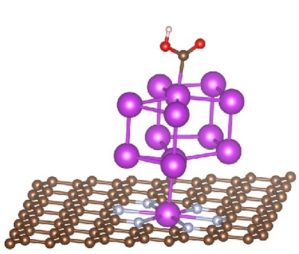	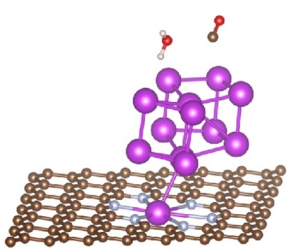	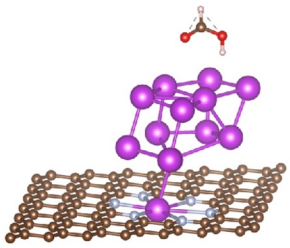
E	-918.12 eV	-921.74 eV	-920.79 eV

Bi N C O H

Fig. S22. Optimized intermediates of Bi@NC for eCO_2R.

	*COOH	*H_2O+*CO	*HCOOH
CONTCAR	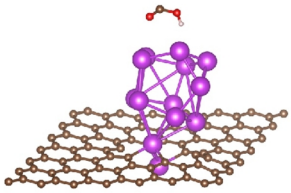	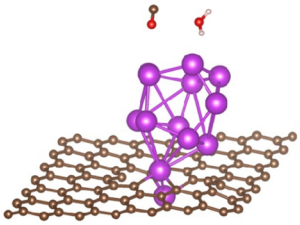	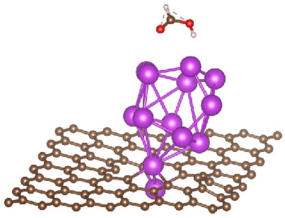
E	-915.25 eV	-919.79 eV	-920.70 eV

Bi N C O H

Fig. S23. Optimized intermediates of Bi@C for eCO_2R.

3 References

1 G. Kresse and J. Furthmüller, *Phys. Rev. B*, 1996, **54**, 11169-11186.

2 J.P. Perdew, K. Burke and M. Ernzerhof, *Phys. Rev. Lett*., 1996, **77**, 3865-3868.

3 P.E. Blöchl, *Phys. Rev. B*, 1994, **50**, 17953-17979.

4 H.J. Monkhorst and J.D. Pack, *Phys. Rev. B*, 1976, **13**, 5188-5192.

5 S. Grimme, J. Antony, S. Ehrlich and H. Krieg, *J. Chem. Phys.*, 2010, **132**, 154104.

6 K. Momma and F. Izumi, *J. Appl. Cryst*., 2011, **44**, 1272-1276.

7 J.K. Nørskov, J. Rossmeisl, A. Logadottir, L. Lindqvist, J.R. Kitchin, T. Bligaard and H. Jonsson, *J. Phys. Chem. B*, 2004, **108**, 17886-17892.

8 Z. Wu, H. Wu, W. Cai, Z. Wen, B. Jia, L. Wang, W. Jin and T. Ma, *Angew. Chem. Int. Ed.*, 2021, **133**, 12662-12667.

9 S. Liu, Y.P. Fan, Y. Wang, S. Jin, M.C. Hou, W.J. Zeng, K. Li, T.L. Jiang, L. Qin, Z.H. Yan, Z.L. Tao, X.H. Zheng, C.Y. Shen, Z.C. Liu, T. Ahmad, K. Zhang and W. Chen, *Nano Lett.*, 2022, **22,** 9107-9114.

10 Y. Wang, L. Xu, L. Zhan, P. Yang, S. Tang, M. Liu, X. Zhao, Y. Xiong, Z. Chen and Y. Lei, *Nano Energy*, 2022, **92,** 106780.

11 Y. Wang, Z. Huang, Y. Lei, J. Wu, Y. Bai, X. Zhao, M. Liu, L. Zhan, S. Tang and X. Zhang, *Chem. Commun*., 2022, **58**, 3621-3624.

12 Y. Chen, Y. Zhang, Z. Li, M. Liu, Q. Wu, T.W.B. Lo, Z. Hu and L.Y.S. Lee, *ACS Nano*, 2024, **18**, 19345-19353.

13 Y. Guan, S.Q. Wu, H.Z. Huang, Z. Zhu, W. Tian and A.X. Yin, *Chem. Asian J.*, 2024, **19**, e202400296.

14 Y. Wang, Y. Li, J. Liu, C. Dong, C. Xiao, L. Cheng, H. Jiang, H. Jiang and C. Li, *Angew. Chem. Int. Ed.*, 2021, 133, 7759-7763.

15 S. Mandal and P. Kumar, *Sustain. Energy Fuels*, 2023, **7**, 4630-4637.

16 C. Yang, Y. Hu, S. Li, Q. Huang and J. Peng, *ACS Appl. Mater. Interfaces*, 2023, **15**, 6942-6950.

17 D. Wang, C. Liu, Y. Zhang, Y. Wang, Z. Wang, D. Ding, Y. Cui, X. Zhu, C. Pan and Y. Lou, *Small*, 2021, **17**, 2100602.

18 L. Zhang, T. Wang, X. Zhang and P. Du, *ACS Sustain. Chem. Eng.*, 2024, **12**, 14070-14076.

19 S. Santra, V. Streibel, L.I. Wagner, N.Y. Cheng, P. Ding, G.D. Zhou, E. Sirotti, R. Kisslinger, T. Rieth, S.Y. Zhang and I.D. Sharp, *ChemSusChem*, 2024, **17**, e202301452.

20 C. Liu, Z. Wu, Y. Li, H. Yu, S. Chen, W. Hong, S. Deng and J. Wang, *New J. Chem.*, 2024, **48**, 15112-15119.

21 Z. Liu, Q. Fan, H. Huo, F. Yao, X. Gao, and J. Wang, *Sci. China Chem.*, 2024, **67**, 2190-2198.

22 Y. Wang, R. Yang, Y. Chen, G. Gao, Y. Wang, S. Li and Y. Lan, *Sci. Bull.*, 2020, **65**, 1635-1642.

23 S. Yang, M. Jiang, W. Zhang, Y. Hu, J. Liang, Y. Wang, Z. Tie and Z. Jin, *Adv. Funct. Mater.*, 2023, **33**, 2301984.

24 Z. Jiang, M. Zhang, X. Chen, B. Wang, W. Fan, C. Yang, X. Yang, Z. Zhang, X. Yang, C. Li and T. Zhou, *Angew. Chem. Int. Ed.*, 2023, **62**, e202311223.